Advances in ICRF Physics and Technology on ASDEX Upgrade

J.-M. Noterdaeme[1,2], V. Bobkov[1], R. D'Inca[1], F.Braun[1], L.Colas[6], P.Dumortier[3], R. Dux[1], H. Faugel[1], H. Fünfgelder[1], L. Giannone[1], D. Hancock[4*], D. Hangan[1*], A. Herrmann[1], T. Huijser[5], S. Huygen[3], A. Kallenbach[1], M. El Khaldi[6*], M. Kocan[1], L. Liu[1], H.W. Müller[1], R. Neu[1], A. Onyshenko[7], Y. Podoba[1], K. Polozhiy[1], F. Pompon[1°], Th. Pütterich[1], V. Rohde[1], E. Würsching[1], E, Wolfrum[1], I. Zammuto[1*], the ICRF Group[1] and the ASDEX Upgrade Team[1]

[1] *Max-Planck Institut für Plasmaphysik, Euratom Association, 85748 Garching, Germany*
[2] *Gent University, EESA Department, B-9000 Gent, Belgium*
[3] *LPP- ERM/KMS, Euratom Association, B-1000 Brussels, Belgium*
[4] *CCFE, Culham Science Center, UK*
[5] *TNO, Delft, the Netherlands*
[6] *CEA, Cadarache, Euratom Association, France*
[7] *Kharkov University, Kharkov, Ukraine*

E-mail contact of main author: noterdaeme@ipp.mpg.de

Abstract. ASDEX Upgrade and its accompanying ICRF (Ion Cyclotron Range of Frequencies) test stands are particularly well suited to advance ICRF towards ITER and beyond.
The ability to operate ICRF on plasmas with strong ELMs has identified shortcomings in the arc detection methods, some of which have difficulties to discriminate between ELMs and arcs. The design and optimization of arc detectors require a precise understanding of the RF arc evolution in transmission lines: the characteristics of such arcs are studied on ASDEX Upgrade and on a test bench to measure their noise, their light intensity and their reflected power. The research on arc detection and the development of arc detectors for ITER ICRF system has also lead to the investigation of plasma emission in the MHz range. By studying the noise generated by arcs in MHz range on ASDEX Upgrade, we discovered that the plasma emitted three types of RF signals with frequencies in this range.
Operation with a metallic wall has made ICRF operation in ASDEX Upgrade, specifically with W coated limiters more difficult. Parallel electric antenna near-fields $E_{||}$ are thought to cause high sheath voltages and sputtering at antenna limiters. Guidelines to reduce these fields, in particular those near the limiters, have been elaborated by near-field calculations with the HFSS code. A modification of existing ASDEX Upgrade ICRF antenna has been designed to test the approach based on the calculations before making more fundamental changes. The modifications include an alteration of the limiters to make them toroidally broader, a change of antenna straps by bias-cutting them such that the plasma-facing strap region is toroidally narrower, and an additional internal shield which carries a large fraction of image currents.
Adjacent antennas in ASDEX Upgrade are connected two by two through 3dB couplers for ELM resilience. The connections have now been modified such that two antennas situated on the opposite sides of the torus and not connected via magnetic field lines can be operated simultaneously. This allows a better characterization of the effect of RF power on the increased potentials on the field lines connected to the antenna and on W sputtering.

1. Introduction

The ICRF system on ASDEX Upgrade (R=1.65m, a=0.5m, b=0.8m, $B_t \approx$ 2-2.5 T, $I_p \approx$ 0.8–1.2 MA) consists of 4 generators (30-120 MHz) with an installed power of 2 MW each, connected 2 by to 2 with 3dB couplers to provide ELMs resilience, 4 two-stub matching systems and 4 two-strap antennas. The ICRF system has coupled 7.2 MW out of 8 MW installed. It has done so under diverted H-mode plasmas with strong ELMs. ASDEX Upgrade has moved to an all-metallic wall, the material of choice for the ITER first wall. The machine has an extensive set of diagnostics, in particular for the edge, which is of major interest for

* funded by EFTS, EnTicE, the Euratom network for Training ion cyclotron Engineers
° funded by GOTP, LITE, Lower hybrid and Ion cyclotron TEchnology

ICRF. The work on ASDEX Upgrade is supported by a number of test stands: one of those, the MXP (Manipulator eXPeriment) is used to investigate arcs.

The design and optimization of arc detectors requires a precise understanding of the RF arc evolution in transmission lines: the characteristics of such arcs are studied on ASDEX Upgrade and on MXP to measure noise, light intensity and reflected power. These parameters are used by the Sub-Harmonic arc detector (SHAD), the optical detector and the GUIDAR (GUIded raDAR) to detect arcing. We report here on the progress made with the SHAD system, and the investigation of plasma emission in the MHz range that resulted from it.

Parallel electric antenna near-fields $E_{||}$ are thought to cause high sheath voltages and sputtering at antenna limiters in ASDEX Upgrade. Guidelines to reduce these fields, in particular those near the limiters, have been elaborated by near-field calculations with the HFSS code. The guidelines imply mainly a minimization of the parallel component of the RF image currents at the toroidally curved poloidal limiters. A low-cost modification of existing ASDEX Upgrade ICRF antenna has been designed to test the approach based on the calculations before making more fundamental higher cost changes.
By modifying the pairing of the antennas to the 3dB couplers, it has become possible to operate two antennas that are situated on the opposite sides of torus (rather than adjacent) and, for sufficiently low q_{95} (typically < 4) those are not connected via magnetic field lines. This allows detailed diagnostics of particular antennas in a wide range of parameters without the influence from adjacent antennas. It has been used to investigate the effect of field line length on the sputtering.

2. Arc detection

The objective assigned to the Arc Detection System for ITER is to detect any RF breakdown that occurs inside the ICRF system and that can damage it. The detection must be as fast as possible to switch off the generator and prevent any damage to the RF components. The objective is simple but rather difficult to implement. What are the RF breakdowns to be detected? How can they be detected? Which amount of energy can damage the system? How fast must the system be shut down before components are damaged? The purpose of the studies carried out on ASDEX Upgrade and on MXP is to clarify those questions and give accurate design specifications.
One pillar of the Arc Detection System is the SHAD; it is based on the fact that an arc is a fast transient (an electron avalanche of the order of the nanosecond) occurring inside the RF system. As such, in the frequency domain, it will excite frequencies up to several hundred MHz. The RF noise excited by arcs is not a wideband transient phenomenon but persists for several microseconds and features discrete frequencies, probably corresponding to resonances with the RF line. To detect those frequencies a band-pass filter eliminates the electronic background noise (typically under 5MHz) and the generator frequency and its modulations by the ELMs (on ASDEX-Upgrade, typically 30MHz+/-5 MHz).
The SHAD System has been operated on ASDEX Upgrade for more than 10 years and has successfully detected the high voltage arcs that are detected by VSWR detectors (detection of the reflected wave generated by the short-circuit of the arc). In addition, it has proven resilient to ELMs perturbations: the reflected power due to the change in coupling of the antenna during ELMs trigger the VSWR detector but not the SHAD.
However, in other cases, detections are triggered which seem not to be caused by arcs. The number of these spurious detections was high enough to jeopardize the use of the SHAD as main arc detector: the too frequent spurious detections which lead to generator tripping

resulted in no more power being injected into the plasma. To understand those unwanted detections, it is necessary to analyze the spurious frequencies and thus the spectrum of the signal acquired by the SHAD. The signal comes from a voltage probe located in the transmission line. To help localising the source of the signal, a second probe is installed inside the vacuum vessel. This probe, located on the high field side near the divertor, is a cross-dipole antenna with a broadband spectrum. The signal processing is based on two Acqiris DC265 digitizing cards (8 bits, 200MS/s, 2MB memory/channel, 4 channels).
One card is used to record the signal when the SHAD system is triggered: 2ms of the signal are recorded before and after the SHAD trigger, at a rate of 250MS/s. The other card is used to have an overview of the frequencies during the whole shot. To cope with the limited amount of memory available (2MB), the digitizer records every 10 ms 1500 points, which are enough to make a FFT and get the spectrum. The result is a set of spectra recorded every 10ms.
Three types of spurious detections we observed: the first type with ICRF heating as the only auxiliary source of power. The second type is when NBI (Neutral Beam Injection) is present, even without ICRF heating. The third type occurs during ELMs.

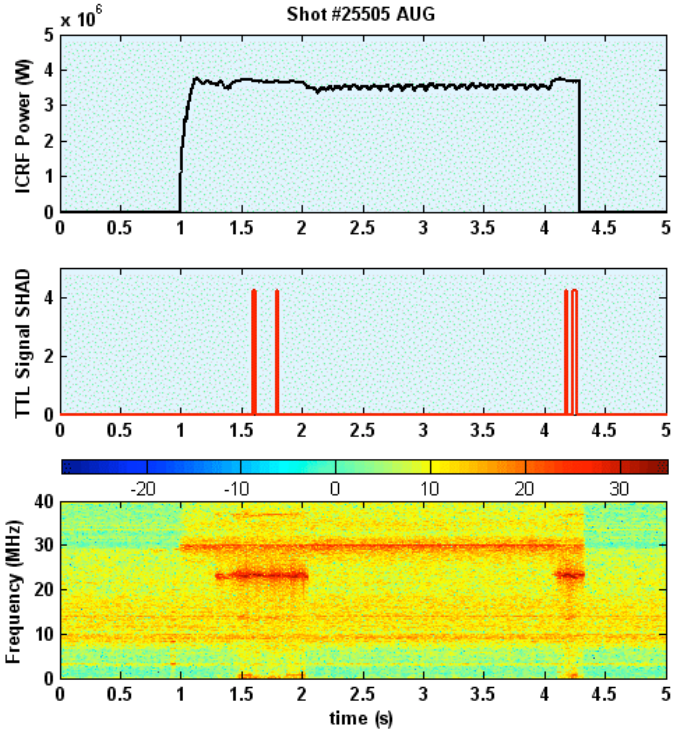

FIG 1. Observation of ICE (Ion Cyclotron Emission) frequency during ICRF heating

Figure 1 shows the ICRF power, the SHAD detections and the signal recorded by the RF probe in the vacuum vessel. A clear frequency appears at about 23MHz with a long duration. The detections occur during the development of the emission at this frequency.
We also recorded the signal both from the RF probe in the vacuum vessel and from the voltage probe inside the ICRF line (the voltage as seen by the SHAD) at the moment of the first detection. The frequency is observed on both probes. Its presence on the voltage probe is the reason for the triggering of the SHAD. The amplitude of the signal from the probe in the vacuum vessel however is higher than in the transmission line, confirming that the plasma is the source of emission. The difference of amplitude seems to be of the order of 20dB but the lack of accuracy on the RF probe calibration leads to high uncertainties of the order of 10dB.

The frequency is detected at low plasma density (<$3.5.10^{19}m^{-3}$ at the edge) and high total RF power (>3MW). The signal depends on the magnetic field but also on the edge plasma density, the evolution of which can cause the chirping of the detected frequencies.
A similar emission has been observed during pure NBI heating. The frequencies observed correspond to the ion cyclotron frequency and harmonics (especially the first harmonic) of Deuterium (or He) at the edge. They are observed for an injected NB power above 8MW.
A last set of observations concerns the first few milliseconds of the injection of a tangential neutral beam in the plasma. A signal is detected at the ion cyclotron frequency in the center during the first 80-100ms of the injection. When the beam is pulsed, the signal reappears at the beginning of each pulse and it is possible to follow its variations in relation with the evolution of the plasma parameters.

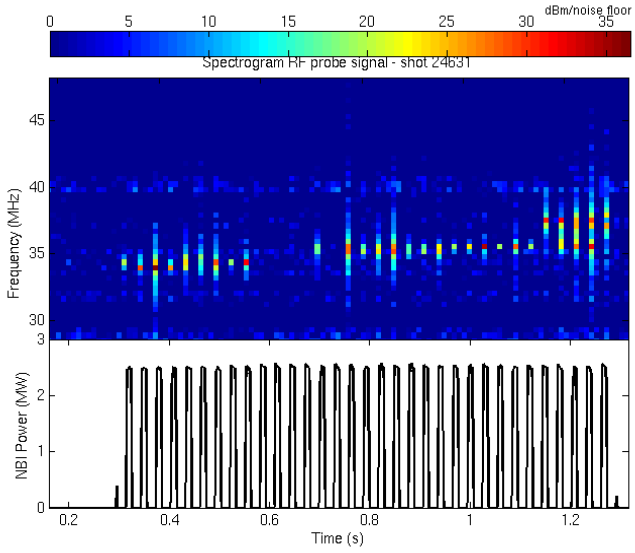

FIG 2. Central Ion Cyclotron Emission during pulsed NBI operations

With steady NBI, the signal can also appear in bursts when a MHD instability is present at the plasma center (sawteeth or fishbones). Although its intensity is too low to affect the SHAD, this phenomenon is under investigation because it could reveal some characteristics of the fast ion distribution in the plasma center. Indeed, the required energy for excitation could come from the inversion of fast ions population before they are scattered to the background thermal ions.
The design of the SHAD will probably have to be modified to remove the perturbations related to ICE. One possibility consists in comparing the signal from the voltage probe of the SHAD with the signal from a RF probe located in the vacuum vessel. The difference in intensities because of the attenuation introduced in each direction by the Faraday shield should indicate the location of the source. All signals, whose origin can be identified as from inside the vacuum vessel, i.e. ICE but also unipolar arcs, can then be ignored by the SHAD.
The improvement of the SHAD system also requires a better understanding of RF breakdowns in frequency domain, more particularly the so-called “low voltage arcs”, the intensity of which is too low to be detected by the present SHAD. Tests on the MXP showed that modifications of the design could help preventing the occurrence of such arcs. Consequently, it would be more a design issue of the RF components than a detection issue.

3. Antenna Design

Operation with the W-wall, in particular with the W-coated limiters and without boronization, has made the use of ICRF power in ASDEX Upgrade more difficult [1]. This is shown in Fig. 3, which presents the evolution of the rise of the edge W concentration [2] ΔC_W due to ICRF power per MW, for all shots including those with accumulation of W in the plasma (cross, continuous line, red) and the shots excluding those with W accumulation (triangle, dashed line, blue). Horizontal lines show median values for each campaign. Thick vertical lines show the steps of W coverage of AUG PFCs [8], thin vertical lines show boronizations. P_{ICRF}=5 MW is routinely achieved in AUG. Since at C_W above 10^{-5} tungsten radiation becomes non-negligible and at C_W=5·10^{-5}, the first limitations of routine ICRF operation due to W release appeared after the installation of the first W-covered limiter and the W-covered horizontal plate at the entrance to the outer divertor [3] (from #19547 on). The effect of the W limiter in comparison with the effect of the horizontal plate at the divertor can be judged from Fig. 4, for a discharge with P_{NBI} = 5 MW in the background and NBI alone later. It shows that the rise of C_W is at least 50% higher when antenna *a4* with the W limiter is powered compared to operation of the antennas *a1*/*a2*, which cope only with the W horizontal plate. Although the W horizontal plate effect is likely to be smaller than the effect of the W limiter, it cannot be completely neglected as a W source, similarly to the W coated upper PSL (passive stabilizing loop) introduced two campaigns earlier (from #16338 on, see Fig. 3) which also connects to ICRF antenna along magnetic field lines. Nevertheless, the ICRF power was routinely applied in AUG operation to avoid W accumulation in the plasma center by central power flux until the first campaign with the full-W wall (2007, from #21495 on). The first campaign with the full-W wall, performed intentionally without any boronization proved to be the most critical for ICRF operation: there is more than a factor of 2 difference in ΔC_W on average between this first campaign and the later ones with boronizations (2008, from #23093 on).

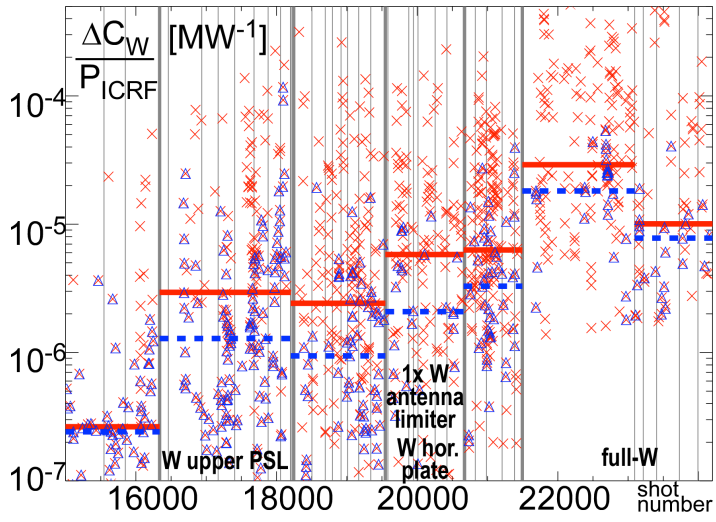

FIG. 3. Long-term evolution of ΔC_W.

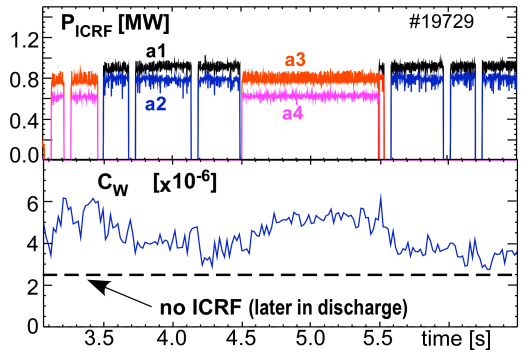

FIG. 4. Comparison of ICRF operation with (a3/a4) and without (a1/a2) W limiter. W limiter is on a4.

Parallel electric antenna near-fields $E_{//}$ are thought to cause high sheath voltages and sputtering at the antenna limiters in ASDEX Upgrade. Guidelines to reduce these fields have been elaborated by near-field calculations with the HFSS code [1]. These imply mainly a minimization of the parallel component of the RF image currents at the toroidally curved limiters. A low-cost modification of existing ASDEX Upgrade ICRF antenna (for its latest

version see Fig. 5) has been designed and built to test the approach based on the calculations before making more fundamental changes with higher costs. The modification includes an alteration of the limiters to make them toroidally broader, a change of antenna straps by bias-cutting them such that the plasma-facing strap region is toroidally narrower, and an additional internal shield which carries a large fraction of image currents. The sheath driving voltages $\int E_{//} \cdot dl$ on the field lines passing in front of the antenna calculated using the HFSS data are a factor of ≈2 lower (Fig. 6) with this new design. To a large extent this is achieved by overall minimization of $E_{//}$. It should be noted that the absolute values of $E_{//}$ and $\int E_{//} \cdot dl$ depend sensitively on the details of geometry surrounding the antenna and on the load and should be treated carefully. The modified antenna will be tested in ASDEX Upgrade at the end of 2010.

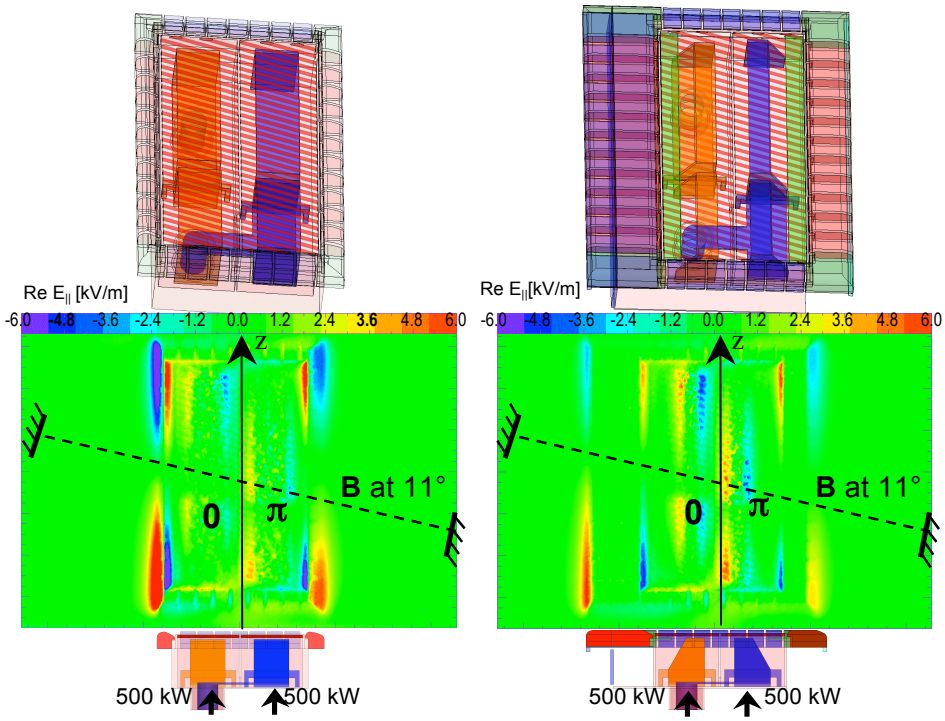

FIG. 5. HFSS $E_{//}$ calculations for original (left) and modified (right) antenna

Adjacent antennas in ASDEX Upgrade are connected two by two through 3dB couplers for ELM resilience. New experimental flexibility with ICRF has been obtained in ASDEX Upgrade by modifying the pairing of the antennas with 3dB couplers. Two antennas that are situated on the opposite sides of torus and are not connected via magnetic field lines for sufficiently low q_{95} (< 4) can now be operated in pair while still using the load resilient 3dB hybrid configuration. This required equalizing the lengths of transmission lines for each antenna and making the connections switchable. Detailed diagnostics of specific antennas in a wide range of parameters without the influence from adjacent antennas has thus become possible. Such a configuration was used to study the ICRF coupling dependence on the location of gas puff in the ASDEX Upgrade vessel reported in [4].

The configuration was also used to characterize the W sputtering patterns on active ICRF antennas. It shows the complexity of the link between the RF drive such as $E_{||}$ and the W sputtering. In Fig. 7 and 8, the W

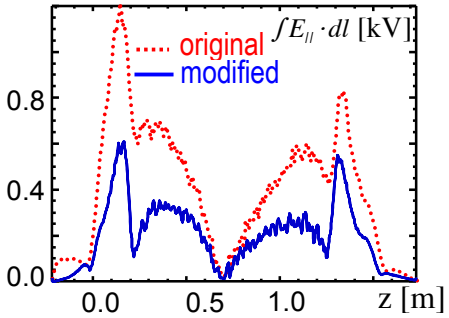

FIG. 6. Comparison of $\int E_{//} \cdot dl$ for original and modified antennas

sputtering pattern evolution, as measured by spectroscopic views of the antenna limiters [1], is shown. The data is taken from L-mode discharges with ICRF heating only, P_{ICRF} = 1.0 MW ≈ *const*, one antenna pair at a time. The density information is provided by the Li-beam diagnostics located next to *a3* at z=0.3 m. The density values in Fig. 7 and 8 correspond to the radial position 3 mm in front of the antenna limiter at z=0.3 m.

In Fig. 7, the vertical z-profiles of tungsten influx, Γ_W, and effective sputtering yield, Y_W, observed at antennas *a3* and *a4* during a scan of the gap between antenna and separatrix ($R_{ant} - R_{sep}$) evolve from peaking below the mid-plane to peaking at the mid-plane. Although no significant global change of magnetic configuration is taking place apart from the shift in plasma position, local changes are dramatic when expressed as changes of connection lengths of a flux tube starting at the spectroscopic spots of observations at *a3* (*a4* has similar changes). The jump in connection lengths correlates with the reversal of the shape of z-profiles of Γ_W and Y_W. There exists a certain correlation between the connection lengths and Γ_W (or Y_W), but the connection lengths taken relatively to each other would not reproduce the z-profile shapes. The change of the plasma position is accompanied by the change in density near the limiter, which could influence the sputtering pattern as well. However the change of density is not a necessary condition for the observed change of the Γ_W and Y_W profiles. In Fig. 8, a similar evolution of the sputtering pattern is shown during a plasma current ramp from 1.02 MA at 1.8 seconds down to 0.9 MA at 2.4 seconds, when the density near the limiter and $R_{ant} - R_{sep}$ stay constant. In this case, the sputtering pattern evolves from being peaked above to below the mid-plane.

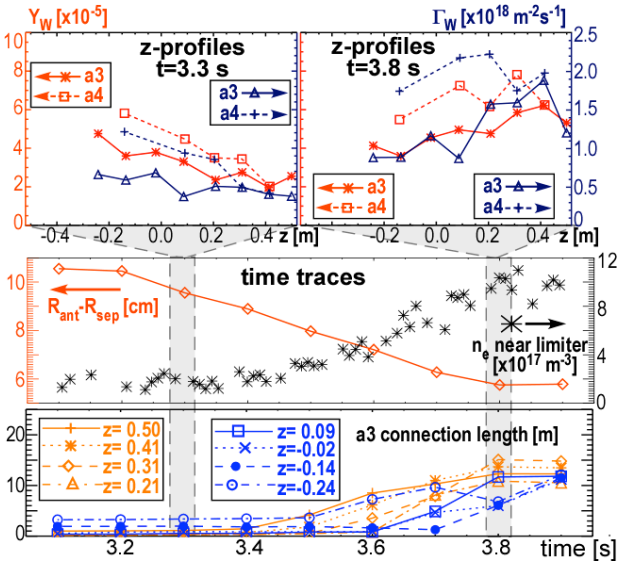

FIG. 7. Evolution of W sputtering pattern (top) during outermost plasma position scan (middle) which results in change of density close to the limiter (middle). Bottom: correlation with evolution of connection lengths of flux tubes starting at the a3 limiter.

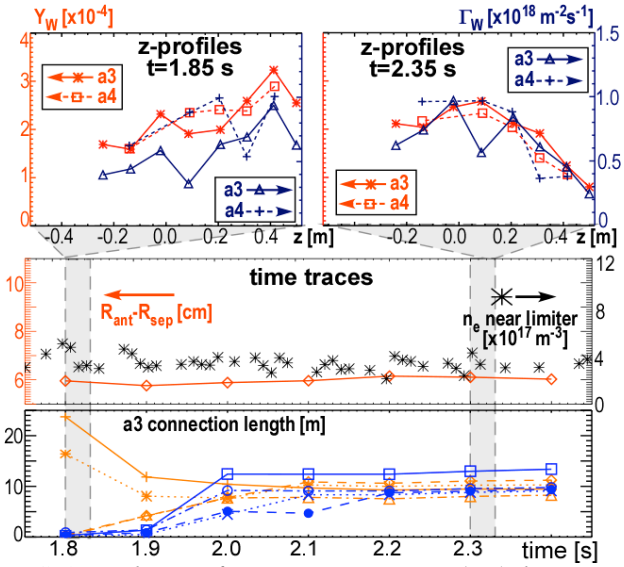

FIG. 8. Evolution of W sputtering pattern (top) during a plasma current scan at constant $R_{ant} - R_{sep}$ (middle) and density near limiter (middle). Bottom: correlation with the evolution of the connection lengths at the a3 limiter.

It has to be noted that spectroscopic observations from Fig. 7 and 8 on *a3* (solid curves) and *a4* (dashed curves) follow the same trends, but a certain difference between the two antennas is observed. The difference is affected by the amount of the gas injected (10^{22} el/s for discharges from Fig. 7 and $3 \cdot 10^{21}$ for those in Fig. 8). It is important to take this into account when comparing two antennas in experiments.

The effect of global magnetic configuration change on ICRF-related W sputtering is demonstrated in Fig. 9. The upper-divertor L-mode discharge #21383

(dashed curves) was repeated in #21384 (solid curves) with the opposite direction of toroidal magnetic field, i.e. the reversed helicity of the magnetic field. The tungsten content in plasma C_W as well as the W influx Γ_W and the effective sputtering yield at limiters Y_W are reduced significantly in #21384. Both discharges were conducted long after boronization (> 150 discharges). Thus it is unlikely that the difference can be explained by virgin boron layers at the limiters being exposed to plasma in #21384, although such effect can not be eliminated completely. On the other hand, one does not expect a decrease of $E_{||}$ and associated sheath driving voltages at the magnetic field misaligned with FS rods by about 20 degrees. Furthermore, JET reported significantly stronger impurity release from the antenna FS with the reversed helicity of magnetic field ([5] and references therein). A more likely explanation of the lower W sputtering at the antenna limiters for the reversed helicity in AUG might lie in the differences in density convection in front of the limiters, such as $E \times B$ convection [6] [7]. Low-frequency spectrograms of fluctuations of ICRF *a3* antenna reflected power (which reacts sensitively on the density profile in front of the antenna) in Fig. 9 (lower part) give an indication of that. The reversed helicity discharge with the low W release is characterized by significantly lower level of fluctuations and gaps without fluctuations at higher P_{ICRF}. Time average coupling characteristics of both discharges show only minor differences.

These experiments indicate that the connection lengths and plasma convection at the ICRF antenna can play an important role independently of the distribution of $E_{||}$ near the antenna. A change of connection length or a change in plasma convection is likely to affect the link between the $E_{||}$ fields, which are thought to drive the sheaths, and the W sputtering yield described in [1]. To obtain a more direct measure of the RF drive of sputtering, poloidal scans for mapping of the plasma potential to an active antenna by probe techniques can be used. The work on the mapping of the potentials in AUG will be described elsewhere.

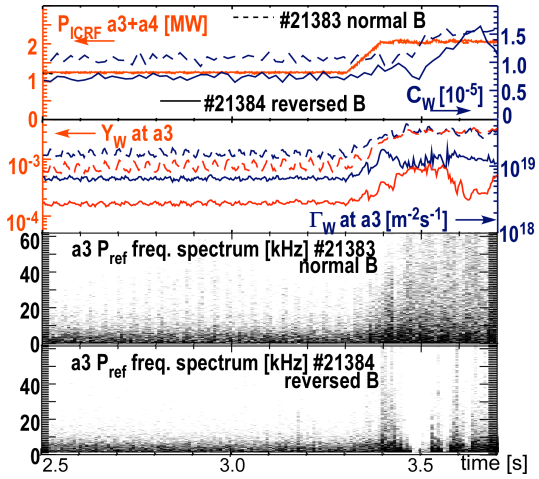

FIG. 9. W sputtering in identical discharges with normal (#21383) and reversed (#21384) direction of toroidal magnetic field

[1] Bobkov, V.V. et al., "*Assessment of compatibility of ICRF antenna operation with full W wall in ASDEX Upgrade*". Nuclear Fusion **50** (2010) 035004.

[2] Pütterich, T. et al., "*Modelling of measured tungsten spectra from ASDEX Upgrade and predictions for ITER*". Plasma Physics and Controlled Fusion **50** (2008) 085016.

[3] Dux, R. et al., "*Plasma-wall interaction and plasma behaviour in the non-boronised all tungsten ASDEX Upgrade*". Journal of Nuclear Materials **390-391** (2009) 858.

[4] Mayoral, M.-L. et al., "*On maximizing the ICRF antenna loading for ITER plasmas*". (2010) ITR/P1-1, this conference.

[5] Dippolito, D.A. et al., "*A Model of Sheath-Driven Impurity Production by ICRF Antennas*". Plasma Physics and Controlled Fusion **33** (1991) 607.

[6] D'Ippolito, D.A. et al., "*Radio-frequency-sheath-driven edge plasma convection and interaction with the H mode*". Phys. Fluids B **5** (1993) 3603.

[7] Colas, L. et al., "*RF current distribution and topology of RF sheath potentials in front of ICRF antennae*". Nuclear Fusion **45** (2005) 767.

[8] Neu, R. et al., "*Operational conditions in a W-clad tokamak*". J. Nucl. Mater. **367–370** (2007) 1497.